Archives of Hydro-Engineering and Environmental Mechanics
Vol. 59 (2012), No. 3–4, pp. 85–100
DOI: 10.2478/heem-2013-0001

VERSITA

A Study on Modelling the Plane Strain Behaviour of Sand and its Stability

Andrzej Sawicki, Justyna Sławińska

Institute of Hydro-Engineering, Polish Academy of Sciences, ul. Kościerska 7, 80-328 Gdańsk, Poland,
e-mails: as@ibwpan.gda.pl, stynaju@ibwpan.gda.pl

(Received October 27, 2011; revised May 25, 2012)

Abstract

The plane strain behaviour of sand is studied using, previously proposed, incremental model describing its pre-failure deformations. Original model has been formulated for the tri-axial configuration, and then generalized for 3D conditions. This 3D model was subsequently adapted to study deformations of sand in the plane strain conditions, in the x_1, x_3 plane. There are three unknowns in such a configuration, namely the principal strains $\varepsilon_1, \varepsilon_3$ and the principal stress σ_2. Respective equations were derived, and then applied to study deformations of sand for chosen stress paths. The governing incremental equations were integrated numerically, and it was shown, for some loading paths, that σ_2 depends linearly on the other principal stresses, so introduction of apparent Poisson's ratio is justified, as a kind of approximation. Subsequent analysis of deformations of sand was performed using this concept, as well as using full system of governing equations.

Key words: sand deformations, liquefaction, instability, plane strain

1. Introduction

This paper deals with the pre-failure behaviour of sand in the plane strain conditions, which are often assumed and analyzed in geotechnical engineering, mostly for practical reasons. In the classical geotechnical literature, 2D models prevail, just to mention the limit or the critical states theories, which are well elaborated, Chen (1975), Derski et al (1988), Schofield and Wroth (1968), Wood (1990). Pre-failure behaviour of sands is usually studied using elasto-plastic models, Lewis and Schrefler (1998), Saada and Bianchini (1989), Zienkiewicz et al (1999), or hypoplastic, Kolymbas (2000), Gudehus (2011). Special approaches are applied to study the phenomenon of soil liquefaction, Jefferies and Been (2006), Lade and Yamamuro (1999).

In this paper, a certain alternative to the above approaches is presented. Subsequent steps of the pre-failure analysis of sand are summarized in Table 1. The starting point is the incremental model of sands' behaviour, originally derived and calibrated for the configuration of triaxial apparatus, Sawicki and Świdziński (2010a, b, c). Then,

these equations were generalized for 3D conditions, using the methods of tensor algebra, Sawicki (2008). These results are summarized in Sections 2 and 3 of this paper. It should be stressed that the incremental model proposed takes into account the initial anisotropy of sand and its initial state, defined either as contractive or dilative. For the triaxial conditions, it describes well the sand deformations before failure and it allows for studying some instabilities of sand.

Table 1. Subsequent steps in the analysis of pre-failure behaviour of sand

Subsequent steps	References
1. Starting point: Incremental model of sand's behaviour before failure, formulated and calibrated for the triaxial configuration (determination of the constitutive functions *M, N, P, Q*).	Sawicki and Świdziński (2010a, b, c). Summary: Sections 2 and 3.
2. 3D generalization of the „triaxial" constitutive equations using the methods of tensor algebra. Determination of the constitutive functions A, B, C, D.	Sawicki (2008). Summary: Sections 2 and 3.
3. Formulation of 3D model for the plane strain conditions in the $\varepsilon_1, \varepsilon_3$ plane. The basic condition $d\varepsilon_2 = 0$ allows for determination of the respective stress increment $d\sigma_2$.	Section 4.
4. Applications include determination of pre-failure deformations for arbitrary loading paths, analysis of instability and liquefaction.	Sections 5, 6, 7.

Then, the model is applied to study the pre-failure behaviour of sand in the plane strain conditions. Respective equations are derived in Section 4, and some applications are presented in subsequent sections. These applications include the analysis of pre-failure deformations of sand and its unstable behaviour. The results obtained, and the proposed methodology, are original and can be used to test the experimental data obtained from the plane-strain tests like, for example, those obtained by Wanatowski and Chu (2006) or Chu and Wanatowski (2009).

The plane strain tests are not so popular in geotechnical engineering as conventional triaxial tests, performed in standard apparatuses, even including advanced equipment, enabling measurement of lateral stresses or propagation of stress waves, and subsequent determination of respective moduli. There is relatively a small number of papers devoted to this important problem, just to mention Alshibli et al (2004), Drescher et al (1990), Finno et al (1997), Han and Vardoulakis (1991), Hettler and Vardoulakis (1984), Lee (1970), Marachi et al (1981) or Tatsuoka et al (1986). These papers, however, do not take into account the phenomena which are described in the present contribution, neither the proposed methodology. The model of soil behaviour, presented in this paper, needs further empirical verifications to be useful for engineer-

ing purposes, however, its structure enables, at least, some fundamental investigations on the pre-failure behaviour of granular soils. The model presented in this paper is not for practical purposes, for its complicated algebra, but it is a good tool for basic investigations.

2. Constitutive Equations

The following incremental equations describe the pre-failure behaviour of granular soils in a general 3D case, see Sawicki (2008):

$$d\varepsilon_v = Adp' + BdJ_2, \tag{1}$$

$$d\boldsymbol{\varepsilon}^{\mathbf{dev}} = \mathbf{C}dp' + Dd\boldsymbol{\sigma}^{\mathbf{dev}}, \tag{2}$$

where: $d(\dots)$ = increment of respective quantity; ε_v = volumetric strain; $\boldsymbol{\varepsilon}^{\mathbf{dev}}$ = deviatoric strain; p' = mean effective stress; $\boldsymbol{\sigma}^{\mathbf{dev}}$ = deviatoric stress: J_2 = second invariant of the stress deviator; A, B, D = constitutive functions; $\mathbf{C}$ = constitutive tensor.

The above constitutive functions are given by other functions, determined from the triaxial experiments:

$$A = M, \tag{3}$$

$$B = \frac{N\sqrt{3}}{2\sqrt{J_2}}, \tag{4}$$

$$D = \frac{3Q}{2}, \tag{5}$$

$$\mathbf{C} = C\mathbf{S}^{\mathbf{dev}},$$

$$C = \frac{3P}{2}, \tag{6}$$

where C = another scalar function, and

$$\mathbf{S}^{\mathbf{dev}} = \frac{1}{3}\begin{bmatrix} 2 & & \\ & -1 & \\ & & -1 \end{bmatrix} \tag{7}$$

is the deviatoric part of the structural tensor, describing the cross-anisotropic properties of granular soils, see Sawicki (2008). The vertical direction x_1 is privileged, as shown by experimental results, cf. Sawicki and Świdziński (2010a).

The symbols M, N, P and Q denote the constitutive functions, determined from the triaxial compression tests, see Sawicki and Świdziński (2010a). The constitutive equations for triaxial conditions are of the following form:

$$d\varepsilon_v = Mdp' + Ndq, \tag{8}$$

$$d\varepsilon_q = Pdp' + Qdq, \tag{9}$$

where:

$$q = \sqrt{3J_2}, \tag{10}$$

$$dq = \frac{\sqrt{3}}{2\sqrt{J_2}} dJ_2, \tag{11}$$

$$\varepsilon_q = \sqrt{\frac{4K_2}{3}}, \tag{12}$$

$$K_2 = \frac{1}{2} tr\left(\boldsymbol{\varepsilon}^{\mathbf{dev}}\right)^2. \tag{13}$$

Eqs. (1) and (2) reduce to (8) and (9) for the case of axi-symmetrical stress and strain states. The functions M, N, P and Q have different shapes for the loading and unloading. The shape of function N also differs for the initially contractive and dilative sand. The definition of loading and unloading differs from that widely adopted in soil mechanics, and is the following:

$dp' > 0$ – spherical loading;
$dp' < 0$ – spherical unloading;
$d\eta > 0$ – deviatoric loading;
$d\eta < 0$ – deviatoric unloading,

where:

$$\eta = \frac{q}{p'} = \frac{\sqrt{3J_2}}{p'}, \tag{14}$$

$$d\eta = \frac{\sqrt{3}}{p'}\left(\frac{1}{2\sqrt{J_2}} dJ_2 - \frac{\sqrt{J_2}}{p'} dp'\right). \tag{15}$$

Tables 2 and 3 summarize the constitutive functions, for the loading and unloading respectively.

Table 2. Constitutive functions for loading, see Eqs. (8) and (9). Initially contractive sand.

Function	Analytical expression
M	$A_v/2\sqrt{p'}$
N	$4c_1\eta^3/\sqrt{p'}$
P	$A_q/2\sqrt{p'}$
Q	$[b_1 b_2 \exp(b_2\eta)]/\sqrt{p'}$

Table 3. Constitutive functions for unloading

M	N	P	Q
$A_v^u/2\sqrt{p'}$	$a_v/\sqrt{p'}$	$A_q^u/2\sqrt{p'}$	$b_q/\sqrt{p'}$

The quantities like $A_v, A_q, c_1, b_1, \ldots$ are just numbers (material's coefficients), and their values will be presented later. As already mentioned, the function N differs from that shown in Table 2 for the initially dilative sand, and is the following:

$$d\varepsilon_v = \frac{\partial \varepsilon_v}{\partial \eta}\frac{\partial \eta}{\partial q}dq = \frac{1}{\sqrt{p'}}(2a_1\eta + a_2)dq = Ndq, \tag{16}$$

for $0 < \eta < \eta'$, and

$$N = \frac{1}{\sqrt{p'}}\left\{\exp(a_6\eta)\left[a_3a_6\eta^2 + (2a_3 + a_4a_6)\eta + a_4 + a_5a_6\right] - 2a_3\eta - a_4\right\} \tag{17}$$

for $\eta' < \eta < \eta''$, where η' corresponds to the instability line (surface), and η'' corresponds to the Coulomb-Mohr failure criterion (assumed as the critical or steady states). Exemplary values of the coefficients a_i will be presented later. The instability line, in the case of triaxial compression is of the following form:

$$q = \Psi p', \tag{18}$$

where Ψ is the coefficient determined from experiments. In the case of triaxial compression tests, there is $\Psi = \eta' = 0.9 \div 1$.

In the 3D case, this equation takes the following form:

$$J_2 = \frac{1}{3}(\Psi p')^2. \tag{19}$$

3. Values of Parameters

The parameters appearing in the constitutive functions M, N, P and Q were determined from the triaxial tests, performed on the model sand "Skarpa", see Sawicki and Świdziński (2010a). Their values were determined separately for the initially contractive and dilative sand, using the following units: **stress unit** 10^5 N/m^2 and **strain unit** 10^{-3}**.** Such units are convenient in numerical calculations, as we deal with numbers of the same order of magnitude. Consider, for example, the uni-axial Hooke's law $\sigma = E\varepsilon$. Let $E = 2 \times 10^8$ N/m^2 and $\varepsilon = 3 \times 10^{-3}$. Substitution of these values into the above equation gives $\sigma = 6 \times 10^5$ N/m^2. It is much more convenient to introduce the values $E = 2$ and $\varepsilon = 3$, and the result of calculation is obviously $\sigma = 6$, but expressed in respective unit. The average values of parameters are listed below.

Loose sand:

$$A_v = 6; \quad A_q = -0.95; \quad A_v^u = 4.4; \quad A_q^u = -0.45.$$

Dense sand:

$$A_v = 3.47; \quad A_q = -0.53; \quad A_v^u = 2.9; \quad A_q^u = -0.21.$$

Initially dilative sand (dense):

$$a_1 = -1; \quad a_2 = 2; \quad a_3 = 4.07 \times 10^{-6}; \quad a_4 = -9.44 \times 10^{-3};$$

$$a_5 = 1.1 \times 10^{-2}; \quad a_6 = 6.54;$$
$$b_1 = 3.5 \times 10^{-4}; \quad b_2 = 6.65; \quad b_q = 0.4; \quad a_v = -0.4.$$

Initially contractive sand:

$$c_1 = 2.97; \quad a_v = -0.87; \quad b_1 = -0.023; \quad b_2 = 6.245; \quad b_q = 0.76.$$

Angles of internal friction:

Loose sand $\varphi = 34^\circ$; $\eta'' = 1.375$; dense sand $\varphi = 41^\circ$; $\eta'' = 1.68$.

Instability line: $\eta' = \Psi = 1$, see Eq. (18).

4. The Plane Strain Conditions

4.1. General Relations

Consider the case shown in Fig. 1, where σ_i; $i = 1, 2, 3$ are the principal stresses. The stress σ_2 is perpendicular to the σ_1, σ_3 plane. The plane strain condition is defined by the following relation:

$$\varepsilon_2 = 0 \quad \text{or} \quad d\varepsilon_2 = 0. \tag{20}$$

The deviator of stress tensor is the following:

$$\begin{aligned} \boldsymbol{\sigma}^{\mathbf{dev}} &= \frac{1}{3}\begin{bmatrix} 2\sigma_1 - (\sigma_2 + \sigma_3) & & \\ & 2\sigma_2 - (\sigma_1 + \sigma_3) & \\ & & 2\sigma_3 - (\sigma_1 + \sigma_2) \end{bmatrix} = \\ &= \begin{bmatrix} \sigma_1^{dev} & & \\ & \sigma_2^{dev} & \\ & & \sigma_3^{dev} \end{bmatrix}. \end{aligned} \tag{21}$$

The same form takes the deviator of strain tensor, when the symbol σ is replaced by ε. The second invariant of the stress deviator, and its increment are the following:

$$J_2 = \frac{1}{2} tr\left(\boldsymbol{\sigma}^{\mathbf{dev}}\right)^2 = \frac{1}{3}\left(\sigma_1^2 + \sigma_2^2 + \sigma_3^2 - \sigma_1\sigma_2 - \sigma_1\sigma_3 - \sigma_2\sigma_3\right), \tag{22}$$

$$dJ_2 = \sigma_1^{dev} d\sigma_1 + \sigma_2^{dev} d\sigma_2 + \sigma_3^{dev} d\sigma_3. \tag{23}$$

Substitution of the above relations into the general constitutive equations (1) and (2) leads to the following system of scalar equations:

$$d\varepsilon_1 + d\varepsilon_3 = A_1 d\sigma_1 + A_2 d\sigma_2 + A_3 d\sigma_3, \tag{24}$$

$$2d\varepsilon_1 - d\varepsilon_3 = B_1 d\sigma_1 + B_2 d\sigma_2 + B_2 d\sigma_3, \tag{25}$$

$$-d\varepsilon_1 - d\varepsilon_3 = C_1 d\sigma_1 + C_2 d\sigma_2 + C_1 d\sigma_3, \tag{26}$$

$$2d\varepsilon_3 - d\varepsilon_1 = C_1 d\sigma_1 + C_1 d\sigma_2 + C_2 d\sigma_3, \tag{27}$$

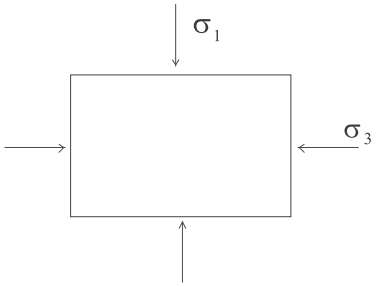

Fig. 1. Principal stresses in the plane strain conditions

where:

$$A_1 = \frac{A}{3} + B\sigma_1^{dev}; \quad A_2 = \frac{A}{3} + B\sigma_2^{dev}; \quad A_3 = \frac{A}{3} + B\sigma_3^{dev},$$

$$B_1 = \frac{2C}{3} + 2D; \quad B_2 = \frac{2C}{3} - D,$$

$$C_1 = -\frac{C}{3} - D; \quad C_2 = -\frac{C}{3} + 2D.$$

There are four equations (24)–(27), but only three unknowns, namely $\varepsilon_1, \varepsilon_3, \sigma_2$. It can be shown that one of these equations depends on the others. If we add Eqs. (24) and (26), the following formula for $d\sigma_2$ is obtained:

$$d\sigma_2 = G_1 d\sigma_1 + G_2 d\sigma_3, \tag{28}$$

where:

$$G_1 = \frac{[-A + C + 3D - B(2\sigma_1 - \sigma_2 - \sigma_3)]}{\Omega},$$

$$G_2 = \frac{[-A + C + 3D - B(2\sigma_3 - \sigma_1 - \sigma_2)]}{\Omega},$$

$$\Omega = A - C + 6D + B(2\sigma_2 - \sigma_1 - \sigma_3).$$

4.2. Changes of σ_2

The first important problem is to examine the changes of σ_2, taking place in the plane strain conditions. In the case of linear and isotropic elasticity, this stress is given by the well known relation:

$$\sigma_2 = \nu(\sigma_1 + \sigma_3), \tag{29}$$

where ν denotes Poisson's ratio, see Timoshenko and Goodier (1951). It can be checked by elementary calculations that this stress is either an intermediate principal stress, or even may take values smaller than remaining two principal stresses.

First, let us examine the changes of σ_2 in the case of anisotropic compression, which means that $\sigma_3 = \xi\sigma_1$, where ξ = const. Note that this parameter should satisfy the following relation:

$$\Phi_1 = \frac{1 - \sin\varphi}{1 + \sin\varphi} < \xi < \Phi_2 = \frac{1 + \sin\varphi}{1 - \sin\varphi}, \tag{30}$$

where φ is the angle of internal friction. Inequality (30) follows from the condition that the stress path should not exceed statically admissible region, bounded by the Coulomb-Mohr limit surface, see Fig. 2.

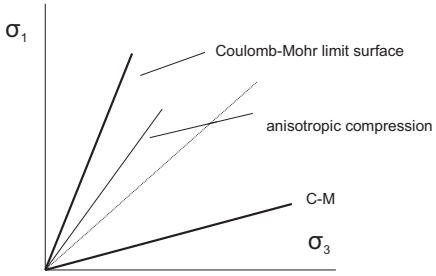

Fig. 2. Anisotropic compression stress path

The stress σ_2 is calculated by integration of Eq. (28). Fig. 3 illustrates σ_2 as function of σ_1 and σ_3, for initially contractive and loose sand, and for $\xi = 1/2$. Interesting conclusion is that this stress changes linearly, although the character of incremental equation (28) is nonlinear. This result suggests that a certain analogy to linear elasticity can be adapted in this case, cf. Eq. (29). Apparent Poisson's ratio is the following: $\nu = 7/(16 + 8) = 0.29$. Such assumption may significantly simplify numerical calculations.

Similar analyses, performed for different values of ξ, also show that σ_2 linearly depends on the other principal stresses. However, values of ν obtained from those calculations slightly differ, as they vary from 0.2 for $\xi = 1$ to 0.38 for $\xi = 3$ and 1/3, i.e. extreme values of ξ, corresponding to stress paths nearly adjacent to the Coulomb-Mohr lines. The following formula approximates quite well numerical results: $\nu = \nu_{\min} + 0.141\ (\ln\xi)^2$. In spite of that, the assumption (29) will be used in further analysis, as the first approximation, in order to simplify calculations.

It should be added that in the case $P = 0$, which corresponds to initially isotropic soil, Eq. (28) give the same result for the anisotropic compression stress paths, symmetric with respect to the $\sigma_1 = \sigma_3$ line in the stress space as it should be.

It is interesting to notice that the stress σ_2 is not necessarily an "intermediate principal stress" as traditionally assumed in the limit states theory. Recall that the Coulomb-Mohr yield condition assumes that such an intermediate principal stress does not influence the limit behaviour of sand. Our analysis shows that σ_2 could be,

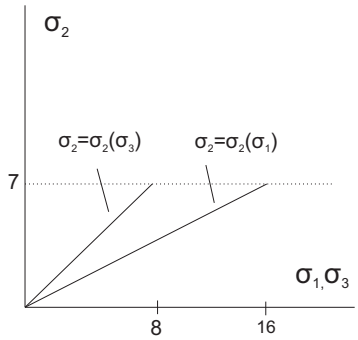

Fig. 3. Changes of σ_2 during anisotropic compression ($\xi = 1/2$) of initially contractive sand

as well, the minor of principal stresses. Assume, for example, that $\nu = 0.29$; $\sigma_1 = 2$; $\sigma_3 = 1$. For these data, Eq. (29) leads to $\sigma_2 = 0.29(2 + 1) = 0.87 < 1$. It seems that this important problem has not been sufficiently investigated in geotechnical engineering.

4.3. Instability Line

Instability surface is given by Eq. (19) which is a generalization of respective expression obtained from the triaxial compression tests, see Sawicki (2008). The second invariant of the stress deviator is given by Eq. (22). In order to simplify the analysis, Eq. (29) will be adapted, which is justified by previous calculations. Eqs. (19), (22) and (29) lead to the following expression:

$$\beta_1 \left(\sigma_1^2 + \sigma_3^2\right) + \beta_2 \sigma_1 \sigma_3 = 0, \tag{31}$$

where

$$\beta_1 = \alpha_1 - \Psi^2 \alpha_3; \quad \beta_2 = \alpha_2 - 2\Psi^2 \alpha_3,$$

$$\alpha_1 = 1 + \nu(\nu - 1); \quad \alpha_2 = 2\nu(\nu - 1) - 1; \quad \alpha_3 = \frac{(1 + \nu)^2}{9}.$$

Eq. (31) represents a curve in the σ_1, σ_3 space. A character of this curve can be determined by well known methods of classical mathematics. For the data corresponding to "Skarpa" sand, i.e. $\nu = 0.29$, $\Psi = 1$, one obtains the pair of straight lines:

$$\sigma_1 = 2.531\sigma_3; \quad \sigma_2 = 0.395\sigma_3, \tag{32}$$

which are symmetrical with respect to $\sigma_1 = \sigma_3$. These lines are situated inside the statically admissible region as $\Phi_1 = 0.32$ and $\Phi_2 = 3.12$, cf. Eq. (30). Note that we have used an average value of ν, see remarks presented in previous sub-section.

The above mentioned symmetry follows from mathematical procedure, and this problem is still not clear from the physical point of view, as the behaviour of soil may

be a little bit different in the triaxial compression and extension tests. The experimental data, quoted in this paper, deal with the triaxial compression tests.

5. Pre-Failure Deformations

5.1. Basic Equations

The starting point are Eqs. (24)–(27). These are four equations for three unknowns, but only three of these equations are independent, which can be checked by addition of Eqs. (25)–(27), after which one obtains the identity. Therefore, one can use arbitrarily only two of these equations, for example (25) and (27). They are equivalent to the following relations:

$$d\varepsilon_1 = S_3 d\sigma_1 + S_4 d\sigma_3, \tag{33}$$

$$d\varepsilon_3 = S_1 d\sigma_1 + S_2 d\sigma_3, \tag{34}$$

where

$$S_1 = -\frac{3}{2}\nu Q; \quad S_2 = \frac{3}{2}(1-\nu)Q; \quad S_3 = \frac{3}{2}(1-\nu)Q + \frac{1+\nu}{2}P; \quad S_4 = -\frac{3}{2}\nu Q + \frac{1+\nu}{2}P.$$

The functions P and Q are defined in Tables 2 and 3, and ν was introduced in Eq. (29), which was supported later by numerical analyses. Note that Eq. (24) was replaced by the assumption (29).

5.2. Deformations During Anisotropic Compression

The anisotropic compression stress path is shown in Fig. 2, and is given by the following relation:

$$\sigma_3 = \xi\sigma_1, \tag{35}$$

where the meaning of ξ was explained in Section 4.2, see Eq. (30). The same relation is valid for the stress increments. In the case (35), Eqs. (33) and (34) take the following form:

$$d\varepsilon_1 = \frac{T_2}{\sqrt{p'}} d\sigma_1; \quad d\varepsilon_3 = \frac{T_3}{\sqrt{p'}} d\sigma_1, \tag{36}$$

where:

$$T_2 = \frac{3}{2}(1-\nu-\xi\nu)T_1 + \frac{(1+\nu)(1+\xi)A_q}{4},$$

$$T_3 = \frac{3}{2}\left[\xi(1-\nu)-\nu\right]T_1,$$

$$T_1 = b_1 b_2 \exp(b_2\eta).$$

The coefficients appearing in the above expressions are defined in Tables 2 and 3, and their values are presented in Section 3 of this paper. The mean effective stress and the non-dimensional shear stress are given by the following relations:

$$p' = \frac{1}{3}(1+\nu)(1+\xi)\sigma_1 = R_1\sigma_1, \tag{37}$$

$$\eta = \frac{\sqrt{3R_2}}{R_1} = \text{const}, \tag{38}$$

where

$$R_2 = \frac{1}{3}\left[\left(1+\nu^2-\nu\right)\left(1+\xi^2\right)+\left(2\nu^2-2\nu-1\right)\xi\right]. \tag{39}$$

Eqs. (36) can be integrated easily, and the following formulae for strains obtained:

$$\varepsilon_1 = \frac{2T_2}{\sqrt{R_1}}\sqrt{\sigma_1}; \quad \varepsilon_3 = \frac{2T_3}{\sqrt{R_1}}\sqrt{\sigma_1}. \tag{40}$$

Fig. 4 illustrates Eqs. (40) for the data corresponding to initially contractive sand, see Section 3 and $\nu = 0.2$. Fig. 5 presents the volumetric and deviatoric strains as functions of the mean effective stress, for the same data. Recall that the deviatoric strain is defined by Eq. (12).

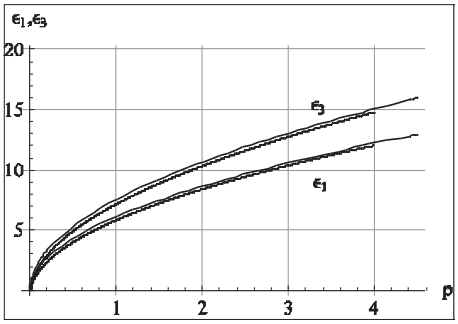

Fig. 4. Principal strains for anisotropic compression, cf. Fig. 2 and Eqs. (40)

The stress-strain relations, shown in Figs. 4 and 5, were determined from Eqs. (24)–(28), which means that they are the exact solution of the problem considered. The stress σ_2, and subsequently the coefficient ν, were also determined from these equations. Then, simplified Eqs. (40) were used to determine the same strains. The results of computations were the same as before, which means that the formulae derived are correct.

5.3. Deformations Caused by Another Simple Loading Path

The next example deals with deformations caused by increasing vertical stress, whilst the horizontal stress remains unchanged (path AB in Fig. 6). It is assumed that

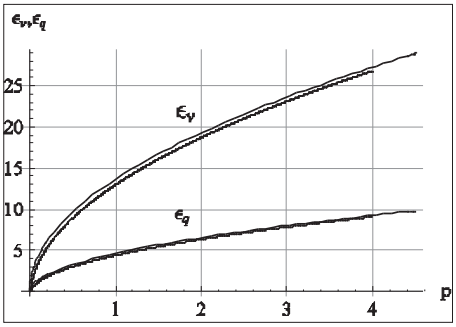

Fig. 5. Volumetric and deviatoric strains as functions of the mean effective stress. Alternative presentation of the results from Fig. 4

the strain state at point A is known. It can be calculated as shown in the previous sub-section or assumed as, for example, the geostatic stress state. On this path, there are only two stress increments, namely $d\sigma_1$ and $d\sigma_2 = \nu d\sigma_1$ as $d\sigma_3 = 0$. The governing equations (33) and (34) reduce to the following form:

$$d\varepsilon_1 = S_3 d\sigma_1; \quad d\varepsilon_3 = S_1 d\sigma_1, \tag{41}$$

where S_1 and S_3 are defined after Eq. (34). Unfortunately, these equations cannot be solved analytically, so numerical procedure should be applied. Figs. 7 and 8 show the results of calculations, for the data from previous example. Fig. 7 shows the changes of principal stresses, and Fig. 8 respective changes of the volumetric and deviatoric strains. Other stress paths, and subsequent deformations, can be analyzed applying the introduced procedure.

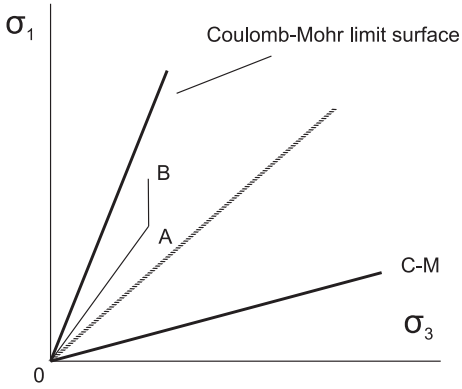

Fig. 6. Exemplary simple loading path

Fig. 9 shows that the horizontal strain decreases along the stress path AB, which physically means expansion of the sample analyzed. This is consistent with intuition. Fig. 9 illustrates the changes of σ_2 along the same path, as function of σ_1. This relation

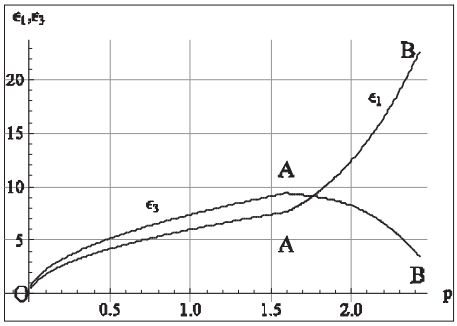

Fig. 7. Principal strains developed along the stress path AB, cf. Fig. 6

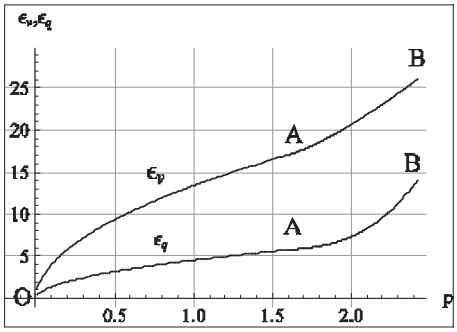

Fig. 8. Volumetric and deviatoric strains along stress path AB. Alternative presentation of the results from Fig. 7

is slightly non-linear, but a linear approximation seems reasonable from the practical point of view.

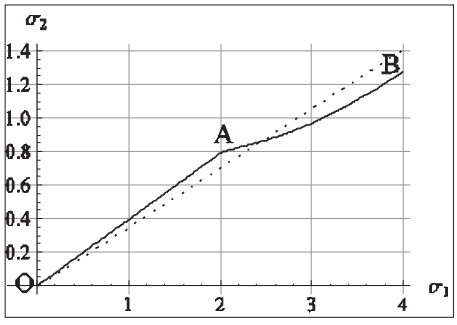

Fig. 9. Changes of apparent Poisson's ratio along stress path AB, see Fig. 6

5.4. Relation between Eqs. (24) and (29)

The above strain-stress relations were derived from Eqs. (25)–(27). It was shown that only two of these equations are independent. Eq. (24) was "replaced" by the assumption (29), and possible consequences of this "replacement" should be analyzed. The main problem is that the constitutive functions S_i depend only on the constitutive functions P and Q. They are independent on the functions M and N, appearing in Eq. (24). The functions M and N describe the volumetric changes of granular soils, due to the respective changes of the mean effective stress and the stress deviator. Replacing of Eq. (24) by the assumption (29) needs some explanations. Some of them were presented in sub-sections 5.2 and 5.3. Recall that the exact solution of the problem analyzed takes into account Eq. (24) in which the functions M and N appear. This full system of equations leads to same results as those obtained from simplified version of governing equations represented by Eqs. (40). Such a result means that the constitutive functions introduced in the description of the triaxial behaviour of sand are dependent. At present, we have not discovered such possible relations.

6. Stability

Hill's condition is used in soil mechanics to study stability of granular materials. It states that a stress-strain state is stable if for all stress and strain increments, linked by the constitutive relations, the second order work is positive, Darve et al (2004). In the plane strain case, considered in this paper, this condition takes the following form:

$$d^2W = d\varepsilon_1 d\sigma_1 + d\varepsilon_3 d\sigma_3 = S_3 d\sigma_1^2 + S_2 d\sigma_3^2 + (S_1 + S_4) d\sigma_1 d\sigma_3 \geq 0, \tag{42}$$

where d^2W denotes the second order work.

In the case of anisotropic compression, considered in sub-section 5.2, the above condition takes the following form:

$$d^2W = \frac{3}{2}(1-\nu)\left(1+\xi^2\right)Q + \left(\frac{1+\nu}{2}\right)(1+\xi)P > 0, \tag{43}$$

as $Q > 0$ and $P > 0$, so the soil behaviour is stable for such stress paths.

In the case of stress path AB shown in Fig. 6, there is $d\sigma_3 = 0$, so the second order work is given by the following relation:

$$d^2W = S_3 d\sigma_1^2. \tag{44}$$

Because $S_3 > 0$, there is also $d^2W > 0$, so the sand behaviour along the path AB is also stable.

7. Discussion and Conclusions

The results obtained in this paper can be summarized as follows:

1. The model enabling studies of the plane strain behaviour of sand in the plane strain conditions is consistent with the requirements of continuum mechanics. It has been calibrated for the tri-axial configuration, and then adapted to analyse 3D conditions, including a special 2D case. There is a lack of direct verification of the results obtained in the plane-strain experimental apparatus, as the Authors have not had access to such devices. However, the model presented is a kind of proposition that can be used to design rational experiments. Published data from such experiments are of a little value for our purposes as those experiments were usually performed randomly. Unfortunately, we have not found, in available literature, the stress-strain curves, which could possibly be used to verify our theoretical results.
2. An important result, obtained in this paper, is that the stress σ_2, perpendicular to the analysed plane of deformations, can be approximated by a simple formula (29), similar to that applied in linear elasticity. Such an assumption significantly simplifies theoretical analyses of the problem, but needs further verifications.
3. The incremental constitutive equations allow for studying the problem of stability of granular soils. It was shown, for exemplary stress paths, that their behaviour is stable. It should be not so in the case of other stress paths.
4. It seems that the proposed constitutive equations have opened some new possibilities to study the pre-failure behaviour of granular soils. Note that such problems, as the liquefaction of saturated sands, have not been included in the analysis presented, as they need a special treatment, but still within the framework proposed.

References

Alshibli A. K., Godbold D. L. and Hoffman K. (2004) The Lousiana plane state apparatus for soil testing, *Geotechnical Testing Jnl*, **27** (4), 1–10.

Chen W. F. (1975) *Limit Analysis and Soil Plasticity*, Elsevier, Amsterdam.

Chu J. and Wanatowski D. (2009) Effect of loading mode on strain softening and instability behavior of sand in plane-strain tests, *Jnl Geotechnical & Geoenvironmental Eng., ASCE,* **135** (1), 108–120.

Darve F., Servant G., Laouafa F. and Khoa H. D. V. (2004) Failure in geomaterials: continuous and discrete analyses, *Computer Methods in Applied Mechanics & Engineering,* 193, 3057–3085.

Derski W., Izbicki R., Kisiel I. and Mróz Z. (1988) *Rock and Soil Mechanics*, PWN/Elsevier, Warszawa/Amsterdam/Oxford/New York/Tokyo.

Drescher A., Vardoulakis I. and Han C. (1990) A biaxial apparatus for testing soils, *Geotechnical Testing Jnl*, **13** (3), 226–234.

Finno R., Harris W. W., Mooney M. A. and Viggiani G. (1997) Shear bands in plane strain compression of loose sand, *Geotechnique*, **47** (1), 149–165.

Gudehus G. (2011) *Physical Soil Mechanics*, Springer, Heidelberg/Dordrecht/London/New York.

Han C. and Vardoulakis I. (1991) Plane-strain compression experiments on water-saturated fine-grained sand, *Geotechnique*, **41** (1), 49–78.

Hettler A. and Vardoulakis I. (1984) Behaviour of dry sand tested in a large triaxial apparatus, *Geotechnique*, **34** (2), 183–198.

Jefferies M. and Been K. (2006) *Soil Liquefaction*, Taylor & Francis, London/New York.

Kolymbas D. (Ed.) (2000) *Constitutive Modelling of Granular Materials*, Springer, Berlin.

Lade P. V. and Yamamuro J. A. (Eds) (1999) *Physics and Mechanics of Soil Liquefaction*, Balkema, Rotterdam/Brookfield.

Lee K. L. (1970) Comparison of plane strain and triaxial tests on sand, *Jnl Soil Mech. Found. Div., ASCE*, **96** (3), 901–923.

Lewis R. W. and Schrefler B. A. (1998) *The Finite Element Method in the Static and Dynamic Deformation and Consolidation of Porous Media*, J. Wiley & Sons, Chichester.

Marachi N. D., Duncan J. M., Chan C. K. and Seed H. B. (1981) Plane-strain testing of sands, [in:] *Laboratory Shear Strength of Soils*, ASTM STP 740, ASTM, Philadelphia, 294–302.

Saada A. and Bianchini G. (Eds) (1989) *Constitutive Equations for Granular Non-Cohesive Soils*, Balkema, Rotterdam/Brookfield.

Sawicki A. (2008) 3D and 2D formulations of incremental stress-strain relations for granular soils, *Archives of Hydro-Engineering & Environmental Mechanics*, **55** (1–2), 45–53.

Sawicki A. and Świdziński W. (2010a) Stress-strain relations for dry and saturated sands. Part I: Incremental model, *Jnl Theoretical & Applied Mechanics*, **48** (2),

Sawicki A. and Świdziński W. (2010b) Stress-strain relations for dry and saturated sands. Part II: Predictions, *Jnl Theoretical & Applied Mechanics*, **48** (2),

Sawicki A. and Świdziński W. (2010c) Modelling the pre-failure instabilities of sand, *Computers & Geotechnics*, **37**, 781–788.

Schofield A. N. and Wroth C. P. (1968) *Critical State Soil Mechanics*, McGraw-Hill, London.

Tatsuoka F., Sakamoto M., Kawamura T. and Fukushima S. (1986) Strength and deformation characteristics of sand in plane strain compression at extremely low pressures, *Soils & Foundations*, **26** (1), 65–84.

Timoshenko S. and Goodier J. N. (1951) *Theory of Elasticity*, McGraw-Hill Book Company, New York/Toronto/London.

Wanatowski D. and Chu J. (2006) Stress-strain behavior of a granular fill measured by a new plane-strain apparatus, *Geotechnical Testing Journal*, **29** (2), 1–9.

Wood D. M. (1990) *Soil Behaviour and Critical States Soil Mechanics*, Cambridge University Press.

Zienkiewicz O., Chan A., Pastor M., Schrefler B. and Simoni T. (1999) *Computational Geomechanics with Special Reference to Earthquake Engineering*, J. Wiley & Sons, Chichester.